# An Extended Climatology for Eyewall Replacement Cycles among Tropical Cyclones in the Western North Pacific

MINGHAO ZHOU
*State University of New York at Albany, Albany, New York*

(19 December 2018)

ABSTRACT

An extended climatology of eyewall replacement cycles (ERCs) among tropical cyclones (TCs) in the Western North Pacific (WNP) was constructed from 1997 to 2017. Based on the different outcome of ERCs, cases were classified into “successful” type and “unsuccessful” type which have different intensity and structure evolution pathways. Environmental modulation on the ERC process was then investigated using TC–relative composite and Empirical Orthogonal Function (EOF) decomposition methods. Preliminary results showed that unfavorable patterns for completing ERCs include higher moisture gradient along the periphery of the TC, dry air intrusion towards the TC center, and TC interactions with upper–level troughs and ridges which will potentially increase vertical wind shear.

## 1. Introduction

Eyewall replacement cycles (ERCs) are common phenomena observed in intense tropical cyclones (TCs). During an ERC, inner rainbands of a TC axisymmetrize to form a secondary eyewall at a larger radius, which robs the original eyewall of moisture convergence and takes over as the new eyewall. Such process is accompanied with significant TC intensity oscillation and structure change, and is important to forecast variations and risk assessments (Houze et al. 2007).

The mechanisms for ERC occurrence are not yet fully understood, while several hypotheses exist. Some ideas favoured ERC initiation as a result of internal TC dynamics, such as the accumulation of outward propagating vortex Rossby wave energy (Montgomery and Kallenbach 1997) and β-skirt axisymmetrization (Terwey and Montgomery 2008). Other research showed that external forcing such as projection from upper-level moist potential vorticity anomaly, interaction with topography or local perturbations in sea surface temperature can also induce secondary eyewall formation via the wind-induced surface heat exchange (WISHE) process (Nong and Emanuel 2003). It is generally acknowledged that environmental factors will to some degree modulate, if not determine, the ERC process.

Sitkowski et al. (2011) used aircraft reconnaissance data from 1977 to 2007 to construct a climatology of TC evolution during an ERC using 24 cases from Atlantic hurricanes. They have found that TCs are generally intensifying when second wind maxima associated with the formation of outer eyewalls are first detected, after which the inner wind maxima weaken as outer wind maxima continue to grow. When the outer eyewall takes over and becomes the primary eyewall, TC can reintensify as the eyewall contracts .The integrated total kinetic energy increases dramatically as a result of a larger eye and broader wind field after an ERC. Similar studies cannot be easily reproduced for other basins due to the lack of in-situ observations, however, with the advent of satellite-borne microwave sensors that can see through the cirrus canopy and reveal the structure of deep convection in TCs (Cecil and Zipser 1997), a large sample pool across the globe has been unveiled.

Many studies have used microwave products to detect and further examine the characteristics of ERCs. Hawkins and Helveston (2004) used concentric rings of brightness temperature in microwave imagery as an identifier, and found that 80% of the TCs exceeding 120 kts in the Western North Pacific (WNP) between 1997 and 2002 undergo ERCs. The WNP has the most number of intense TCs as well as the highest percentage of ERC occurrence, probably because TCs can stay in favourable environment and maintain high intensity for a longer period of time, compared to other basins. Kuo et al. (2009) used a similar approach and identified 62 ERC cases in the WNP between 1997 and 2006, but they found only half of the cases follow the classic "intensify – weaken – reintensify" pattern of TC intensity change during an ERC. Yang et al. (2013) studied 95 ERC cases between 1997 and 2011 and concluded ERCs that last longer have larger outer eyewalls and more vigorous convective activity, while ERCs that did not complete (the outer eyewall dissipated within 20 hours of formation) are on average situated within less favourable environment. The idea of potential environmental modulation on ERC formation was also illustrated by Kossin and Stikowski (2009) by implementing a probabilistic forecasting model based on the Statistical Hurricane Intensity Prediction Scheme (SHIPS), which turned out to be more promising than climatology.

Since the ERC involves a series of TC structure and intensity changes, being able to complete it step by step is what a standard definition demands. In this study, we will dichotomize ERC cases into two scenarios: "successful ERCs" and "failed ERCs" or unsuccessful ERCs, depending on whether the replacement of initial eyewall is completed. Since the average time span for an ERC is 36 hours

(Sitkowski et al. 2011), it is reasonable to hypothesize certain larger-scale environmental factors will exert influence on this process. No previous work has been done regarding the spatial structure of certain environmental field surrounding a TC undergoing an ERC, to the author's knowledge, so we will retrieve, composite and decompose such patterns regarding two different scenarios. An extended climatology for ERCs in the WNP was first constructed first using subjective identification. Section 2 will describe the data and methods used to construct such a catalogue. Summaries of the ERC cases and differences between the two scenarios will be discussed in Section 3. Conclusions of preliminary findings will be addressed in Section 4.

## 2. Data and methodology

Microwave imagery archive from the Navy Research Laboratory (NRL) TC webpage was used for ERC detection (https://www.nrlmry.navy.mil/TC.html). TCs in the WNP from 1997 to 2017 were investigated in this research. Products from multiple sensors were examined subjectively in terms of how "concentric" the brightness temperature rings appear in each image, if any. A brief description of some parameters of the microwave instruments can be found in the work by Wimmers and Velden (2007).

There is no formal definition of what marks the starting time and ending time of an ERC, meanwhile discretion and consistency were of our primary concern for yielding results as objective as possible. The onset of both successful and failed ERCs are determined by the formation of concentric rings on these images. Successful completion of an ERC is defined as the inner eyewall being completely replaced by the outer eyewall, while failure to complete an ERC is defined as either the outer eyewall, or both eyewalls, dissipated halfway. Fig. 1 gives an example of a successful ERC of Typhoon Atsani (2015) and Fig. 2 shows an example of a failed ERC of Typhoon Lekima (2013). Once detected, time frame of the image was converted to the nearest 6-hourly interval for subsequent analysis.

Best track data from Joint Typhoon Warning Center (JTWC) was used to retrieve TC location and intensity (http://www.metoc.navy.mil/jtwc/jtwc.html). Regular data interval is 6 hourly, with occasional 3-hourly special records. ERA-Interim Reanalysis data on N128 Gaussian grid, which is at approximately 0.7 degree resolution, was used to retrieve relative humidity (RH), geopotential height (Z), zonal and meridional wind (U and V wind) field corresponding to the times of ERC onset and completion. The data was then extracted using a TC–centered box in aid of performing composite analysis and Empirical Orthogonal Function (EOF) analysis.

## 3. Results

In the past 21 years, 117 TCs in the WNP undergo a total of 174 ERCs using our criteria, with some TCs undergoing more than one ERC. A complete catalogue of all ERC cases identified, as well as some TC–centered map plots can be found at this website: http://www.atmos.albany.edu/student/mz198736/ERCcases.php . This website will also be updated in real time once further research outcomes are available.

Time series of annual numbers of TCs undergo ERC and number of ERC cases are presented in Fig. 3. These numbers also seem to be highly correlated with the number of intense TCs in each year (not shown), which is not surprising as ERCs typically take place in intense storms. The entire ERC lasts 16 hours on average, ranging from 6 hours to 54 hours. This result is consistent with findings from Stikowski et al. (2011) that the duration of an ERC is shorter when identified using microwave imagery, as well–defined concentric rings appear after the actual formation of secondary wind maxima.

92 out of the 174 cases are successfully completed (52.9%), while the rest 82 cases failed (47.1%). Locations of the onset and termination of ERCs are marked accordingly in Fig. 4 (current plot showing cases from 1997 to 2015; will be updated soon). Successful ERCs are mostly located along the northern edge of the warm pool and over the Kuroshio Current, with an average starting location of 19.0°N, 137.8°E and ending location of 20.4°N, 136.2°E. Average TC intensity at the starting and ending time of the ERC are 116.0kts and 114.6kts, respectively, indicating an unsubstantial maximum intensity change during the ERC.

Failed ERCs are generally located at a slightly higher latitude, or closer to land, though some of them are collocated with successful cases. Among these 82 cases, 29 are associated with TC landfall, and the other 53 take place over the ocean. We will focus on these 53 cases without land intervention from now on. Their average location at onset is 21.5°N, 140.2°E, which shifts to 23.7°N, 140.2°E when ERCs cease. Average TC intensity drops from 116.7 kts to 100.5 kts under this scenario, as many TCs are not able to reintensify if being interrupted during the ERC. The difference between two ERC scenarios is substantial, and it is worthy of digging into more details what is different in terms of environmental patterns that modulates the ERC processes.

*a. Lower–level moisture field pattern difference*

850–700hPa average RH within 15° of the TC center was chosen as a parameter representing lower–level moisture field of and around a TC. Composites of RH field normalized by domain average for successful and failed ERCs at their onset and termination, as well as the difference fields, are shown in Fig. 5. One can see the TC circulation becomes more axisymmetric during successful ERCs, while in failed ERCs the TC is being stretched or sheared to the northeast. Area of relatively dry air both present in two scenarios, while in failed cases the air to the TC's northwestern quadrant is much drier. Moist area associated with inner core convective activity is actually larger in failed ERCs. The difference field suggests that despite smaller high moisture region near TC inner core, successful ERCs are located within moister ambient environment especially 4–8° away from the TC center. RH gradient is higher in failed ERCs as a result of combined higher inner core RH and drier surrounding environment.

Using the EOF decomposition of the RH correlation field, the distribution pattern of relatively moister and drier air centered around a TC were filtered out to some extent. For successful ERCs, the first three EOF spatial modes at the onset and completion of the process are presented in Fig. 6, which can add up to explain about 30% of the total variance. Since the RH field for each individual case contains many smaller–scale features, for example, TC size and rainband/moisture transportation configuration varies greatly between different cases, it can be understood that the percentage of variance explained by leading EOF modes are not particularly high. Rather, the first three patterns passed the significance test recommended by North et al. (1982) and are significantly separated from one another, so they are of value representing some of the spatial patterns. The first mode roughly represents higher RH within the TC circulation itself and lower RH in the surrounding. The second mode depicts higher RH area elongating from the TC center to the northeast, while air of lower RH is located to the northwest of the TC and trying to wrap in from the west. The third mode represents moisture transport from the lower latitudes, and probably some outward propagating rainbands as the ERC proceeds, both setting for a moist environment 4–8° away from the TC center.

Similar EOF decompositions for failed ERCs are shown in Fig. 7, except the third mode for the termination of the event is not significantly separated from the second mode, which requires caution when interpreting. These modes add up to explain 32.7% – 36.4% of the total variance. The first mode still represents the major TC circulation pattern, which is now less axisymmetric and being significantly sheared to the northeast compared to the first mode of successful scenario. The second mode has the bulk of drier air to the north of the TC being wrapped into TC inner core from the southwestern quadrant, and sharper moisture gradient along the outer periphery of the dry tongue. The third mode has a larger, less compact TC circulation with dry air wrapping in from the south, and losts axisymmetricity with time. In general, failed ERCs cases tend to have less axisymmetric TC inner core that may be experiencing higher shear, and more detrimental dry air intrusion into the TC center.

*b. upper-level synoptic flow pattern difference*

200hPa Z field along with U, V wind field within 20° of the TC center are used to examine the difference of upper–level synoptic flow pattern for successful and failed ERC scenarios. From previous results, we can see that TCs that fail to complete an ERC are typically located at higher latitudes, tend to have larger moisture gradient to its northwest, and exhibit shapes indicative of higher shear. More interactions between the TC and mid–latitude systems are hypothesized as a causation. Composite maps as well as the difference fields are shown in Fig. 8, where we do see a deeper trough approaching the TC from the northwest with a jet streak setting up to the TC's northeast. This is an unfavourable pattern for TC development, or a "bad" type of TC–trough interaction, according to personal conversations with Dr. Brian Tang and Dr. Kristen Corbosiero and their sharing some of the recent works with graduate student Casey Peirano in the State University of New York at Albany.

Decomposition of the upper–level pattern into three leading EOF modes using the covariance matrix is presented in Fig. 9 and Fig. 10. The feature associated with synoptic systems are now at a larger scale, so patterns are smoother and better retained. For successful ERCs, these modes can explain roughly 72%, 55%, 92% of the total variance in U, V, Z field, respectively, and similar statistics are 75%, 65%, 93% for failed ERCs. The EOF modes of U, V wind are then artificially combined to yield vector direction and magnitude modes.

The first mode of both scenarios are dominated by a trough located to the northwest of the TC, while the trough associated with unsuccessful ERCs dipping deeper and jet streak ahead of the trough further elongated. The second mode of successful ERCs resemble a jet–entrance–region type configuration, while for failed ERCs mode two depicts a southwestward bending ridge of the upper–level high which imposes more easterly shear on the TCs. The third mode in both scenarios have a separated high pressure system located to the northwest of the TC, which is likely linked to the South Asian High, and it is displaced more equatorward in failed ERC cases owing to a deeper upper–level trough to the north. Such upper level high pressure systems in the WNP are typically associated easterly jets that can bring significant shear to TCs. Using the EOF mode for geopotential height field to derive corresponding geostrophic wind field instead of combining EOF modes for original wind components may be a better way of conveying such information, as the EOFs for three different variables are not necessarily physically connected, according to a personal conversation with Dr. Brian Tang. Further work will be carried out in the future for more convincing results.

## 4. Conclusions

An extended climatology for ERC events in the WNP was constructed. ERC cases were separated into successful ones and interrupted ones, and corresponding environmental patterns were retrieved and compared. By analysing the lower–level moisture field and upper–level dynamic field, differences between the two ERC scenarios were compared and contrasted. Preliminary results showed that:

(1) Successful ERCs take place in TCs that are more axisymmetric and located within moister ambient environment. Higher moisture gradient between the TC inner core and 4–8° away from the TC center is unfavourable for ERC process. Dry air intrusion exists in both scenarios, while it can penetrate through the TC inner core in failed ERCs with the aid of larger gradient and higher shear, despite potentially more vigorous convective activity near the TC center.

(2) Upper–level flow configuration in the two bins of ERC cases are also different. Interacting with a deeper trough to the TC's northwest and a more elongated jet streak to its north is unfavourable for ERC completion, as well as being steered by strong upper–level high pressure systems. Successful

ERCs appear to take place under less interaction with these larger–scale systems.

It should be kept in mind that these patterns are not sufficient for determining whether or not an ERC can be successfully completed, as variability across all cases are large. Nevertheless, this study can offer some new aspects on how TC–environment interactions have modulation on the ERC process. Further research is needed to extract more informative patterns that can help better guide operational forecasts of TC intensity and structure oscillations during an ERC.

## REFERENCES


Cecil, D. J., and E. J. Zipser, 1999: Relationships between tropical cyclone intensity and satellite-based indicators of inner core convection: 86-GHz ice-scattering signature and lightning. *Monthly Weather Review*, 127, 103–123.

Hawkins, J. D., and M. Helveston, 2004: Tropical cyclone multiple eyewall characteristics. *Preprints AMS 26th Hurricane and Tropical Meteorology Conference*, 276–277.

Houze, R. A., S. S. Chen, B. F. Smull, W.-C. Lee, and M. M. Bell, 2007: Hurricane intensity and eyewall replacement. *Science*, **315,** 1235–1239.

Kossin, J. P., and M. Sitkowski, 2009: An objective model for identifying secondary eyewall formation in hurricanes. *Monthly Weather Review*, **137,** 876–892.

Kuo, H.-C., C.-P. Chang, Y.-T. Yang, and H.-J. Jiang, 2009: Western North Pacific typhoons with concentric eyewalls. *Monthly Weather Review*, **137,** 3758–3770.

Montgomery, M. T., and R. J. Kallenbach, 1997: A theory for vortex Rossby-waves and its application to spiral bands and intensity changes in hurricanes. *Quarterly Journal of the Royal Meteorological Society*, **123,** 435–465.

Nong, S. Y., and K. Emanuel, 2003: A numerical study of the genisis of concentric eyewalls in hurricanes. *Quarterly Journal of the Royal Meteorological Society*, **129,** 3323–3338

North, G. R., T. L. Bell, R. F. Cahalan, and F. J. Moeng (1982): Sampling Errors in the Estimation of Empirical Orthogonal Functions. *Monthly Weather Review*, **110,** 699-706.

Sitkowski, M., J. P. Kossin, and C. M. Rozoff, 2011: Intensity and structure changes during hurricane eyewall replacement cycles. *Monthly Weather Review*, **139,** 3829–3847.

Terwey, W. D., and M. T. Montgomery, 2008: Secondary eyewall formation in two idealized, full-physics modeled hurricanes. *Journal of Geophysical Research*, **113,** D12112, doi:10.1029/2007JD008897.

Wimmers, A. J., and C. S. Velden, 2007: MIMIC: A new approach to visualizing satellite microwave imagery of tropical cyclones. *American Meteorological Society*, **88,** 1187–1196.

Yang, Y.-T., K.-C. Kuo, E. A. Hendricks, and M. S. Peng, 2013: Structural and Intensity Changes of Concentric Eyewall Typhoons in the Western North Pacific Basin. *Monthly Weather Review*. **141,** 2632–2648.

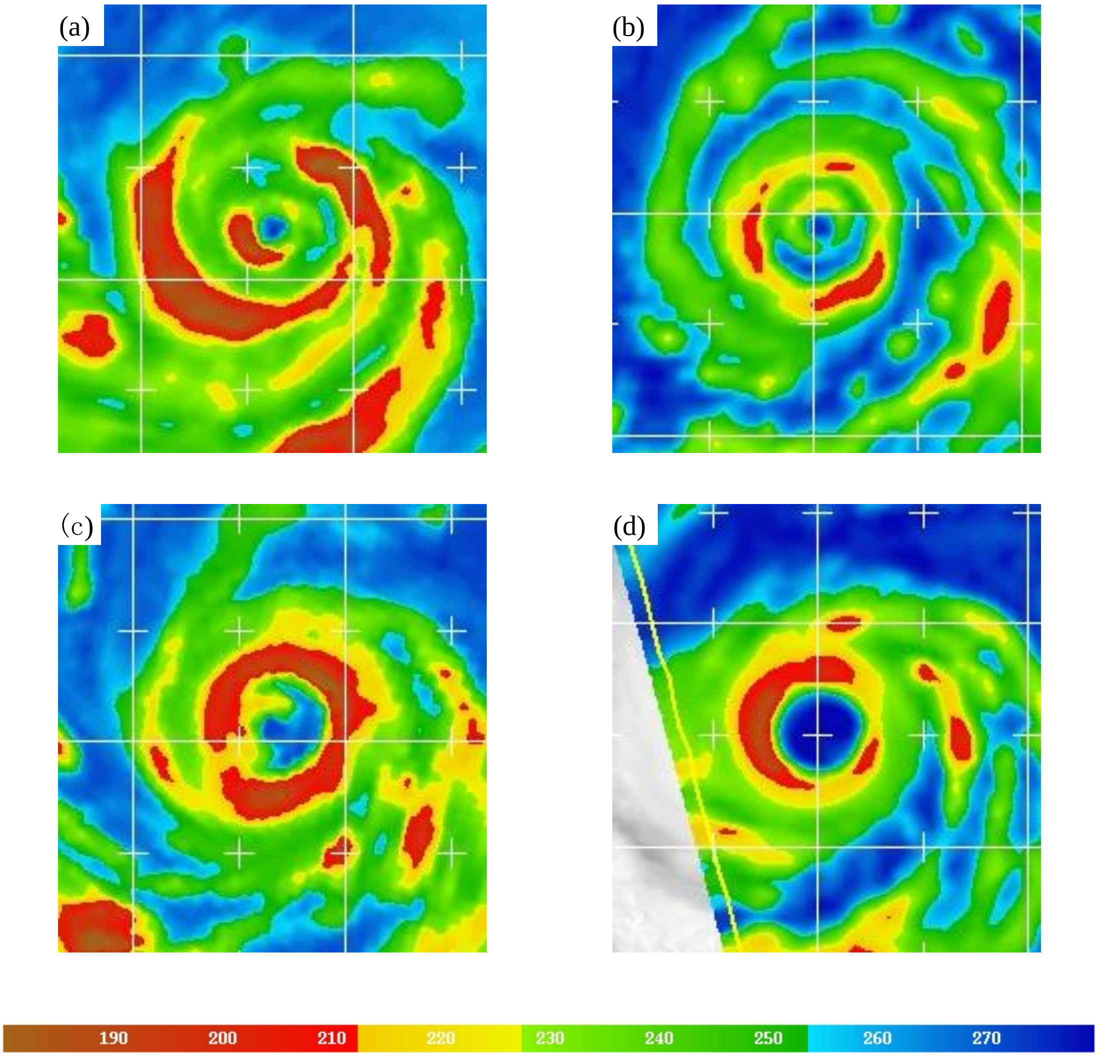


Figure 1. Example of a successful ERC in Typhoon Atsani (2015), images from the NRL website. (a) Secondary eyewall formation (08/18 07:45Z, SSMIS, F19) (b) Onset of the ERC (08/18 16:46Z, SSM/I, F15) (c) Inner eyewall dissipation (08/18 20:19Z, SSMIS, F19) (d) Completion of the ERC (08/19 03:59Z, SSM/I, F15)

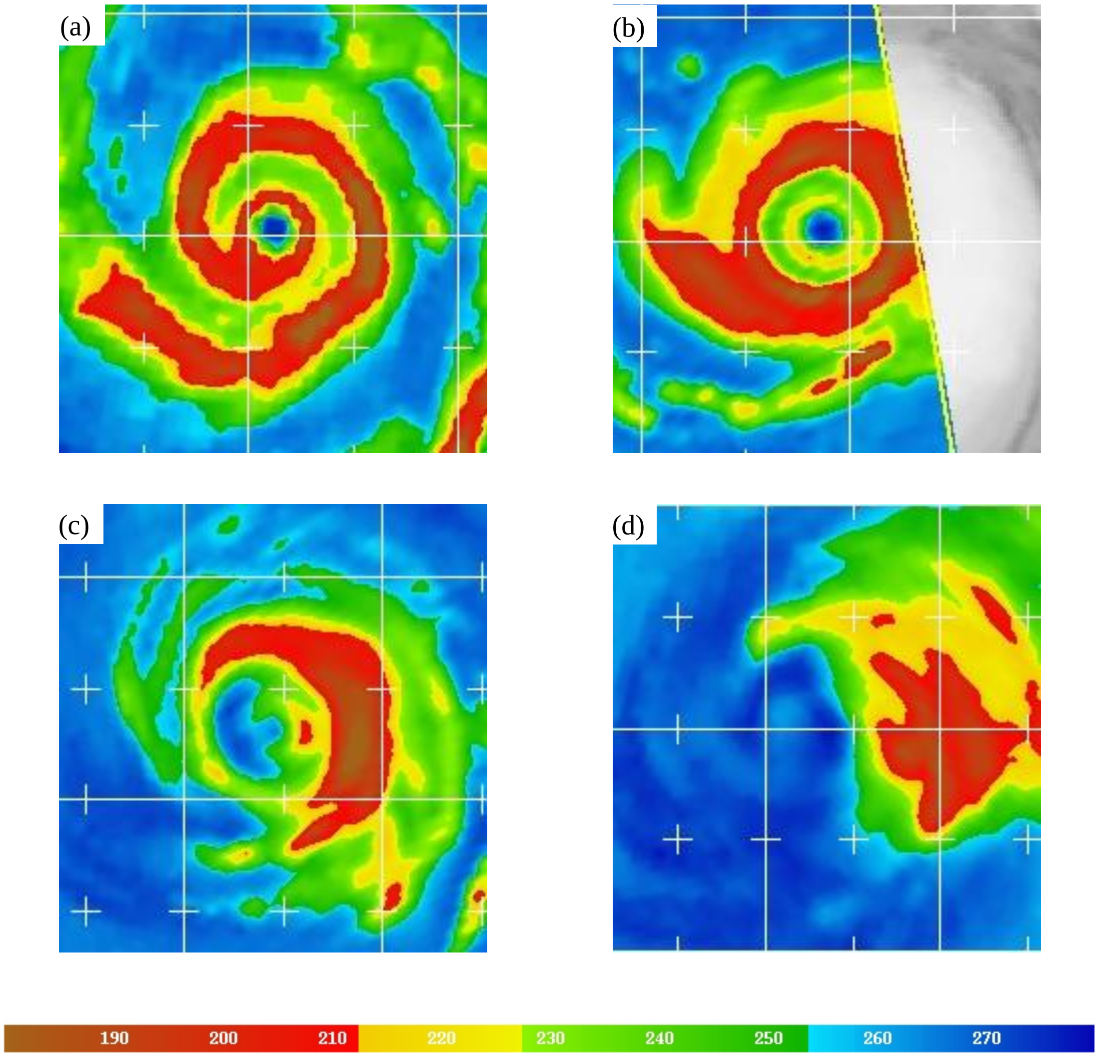


Figure 2. Example of a failed ERC in Typhoon Lekima (2013), images from the NRL website. (a)Secondary eyewall formation (10/23 20:19Z, SSMIS, F17) (b) Onset of the ERC(10/24 10:32Z, SSMIS, F18) (c) Inner eyewall dissipation (10/25 10:22Z, SSMIS, F18) (d) Termination of the ERC as both eyewalls dissipated (10/25 22:47Z, SSMIS, F18)

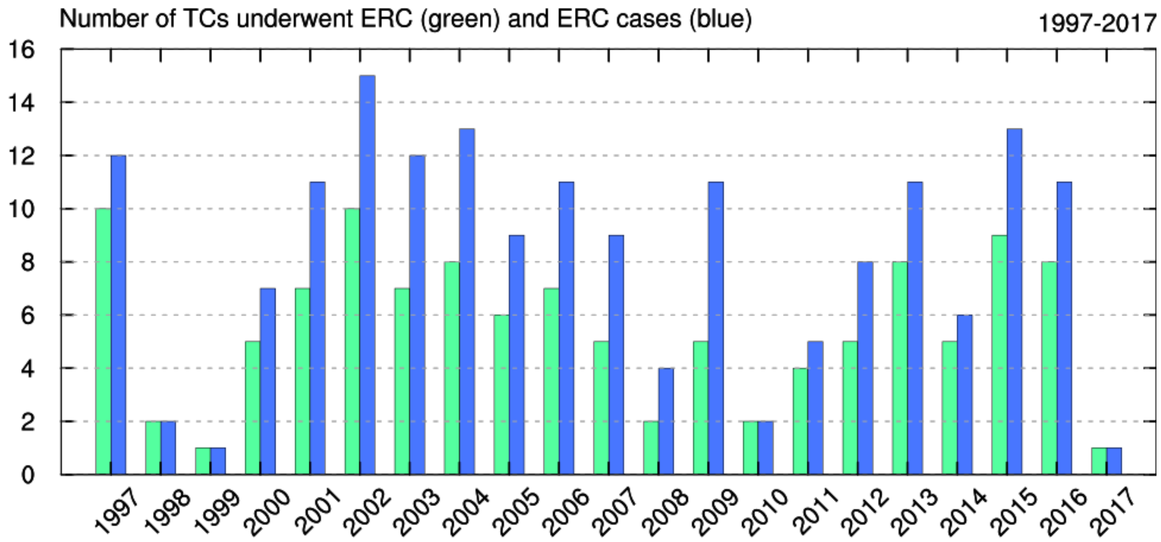


Figure 3. Time series of TCs undergo ERC and number of ERC cases per year from 1997 to 2017.

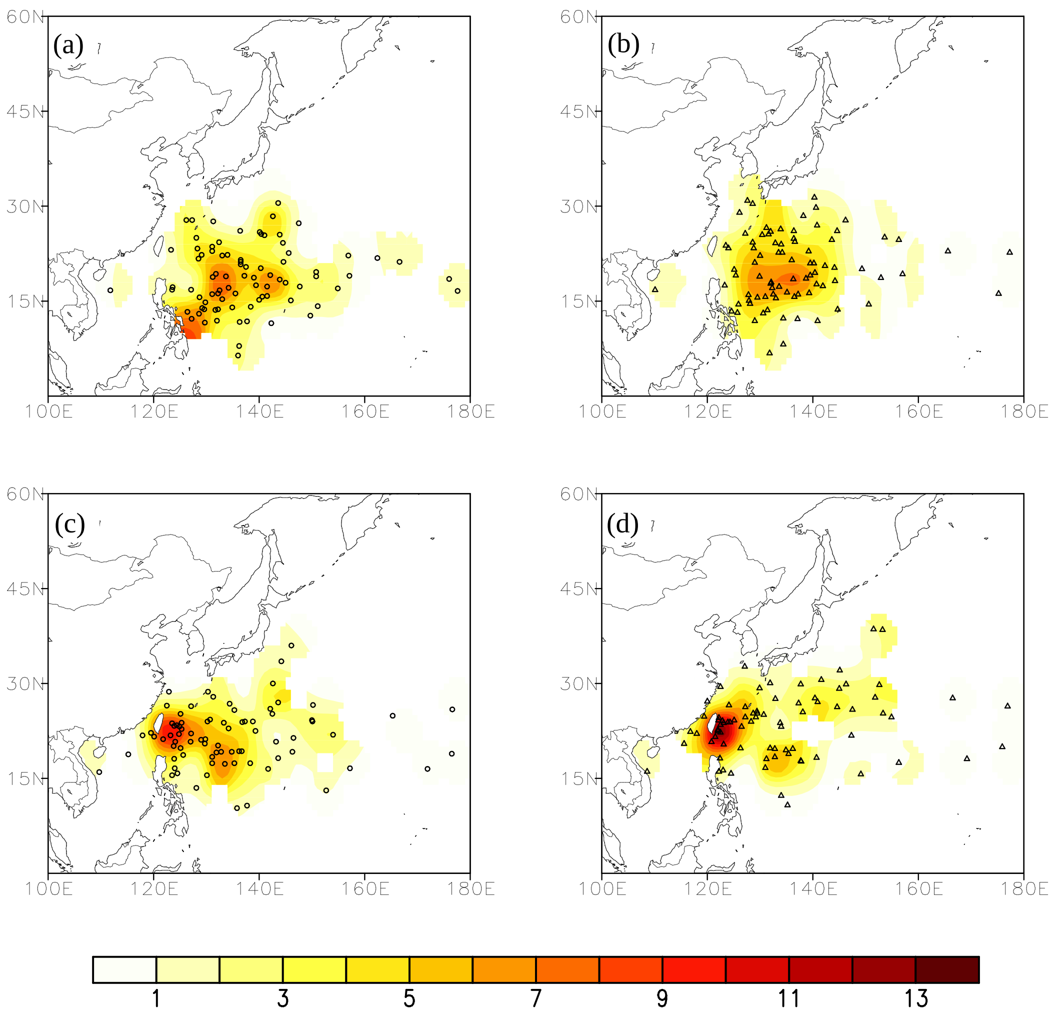


Figure 4. Locations and frequencies for (a) onset of successful ERCs, (b) completion of successful ERCs, (c) onset of failed ERCs, and (d) termination of failed ERCs. (Cases currently showing are between 1997 and 2015.)

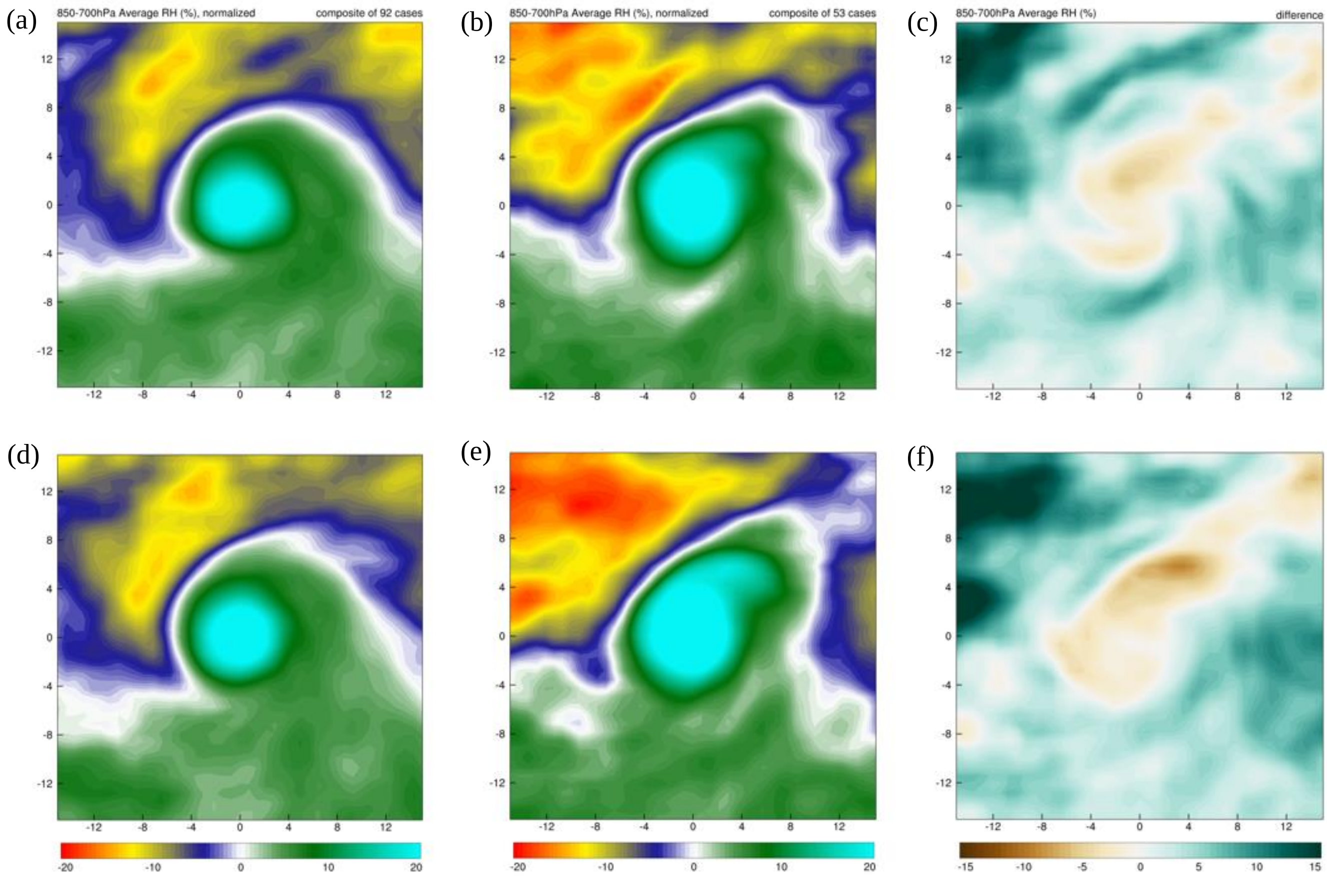


Figure 5. Composite maps of normalized 850–700hPa RH (%) within 15°×15° relative to TC center, for (a) onset of successful ERCs, (b) onset of failed ERCs, (d) completion of successful ERCs, (e) termination of failed ERCs. Plots on the rightmost panel are difference fields of success cases minus failed cases at (c) ERC starting time, and (f) ERC ending time.

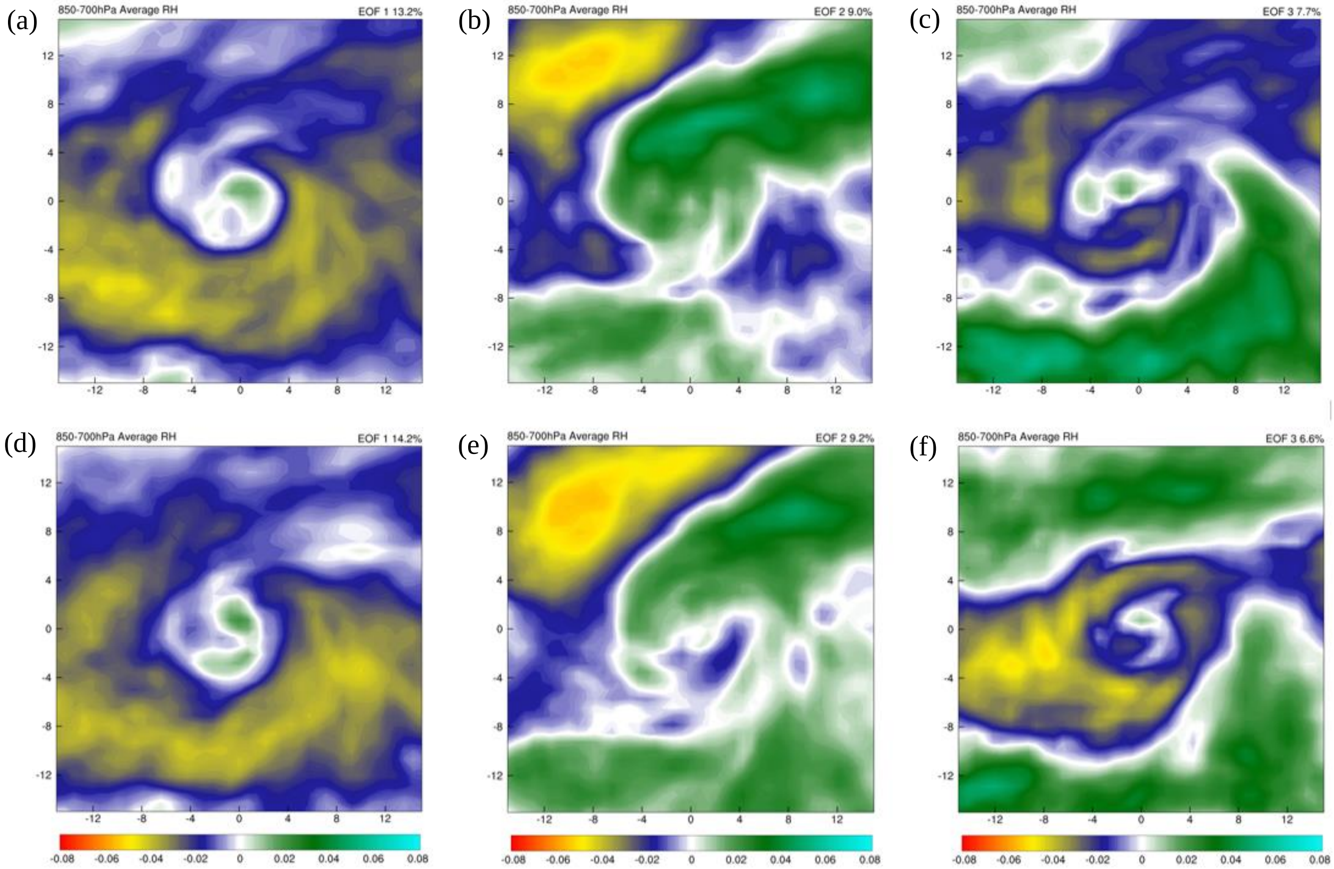


Figure 6. RH field EOF mode 1, 2, 3 for (a) ~ (c) onset of successful ERCs, and (d) ~ (f) completion of successful ERCs, respectively.

(a) (b) (c) (d) (e) (f)

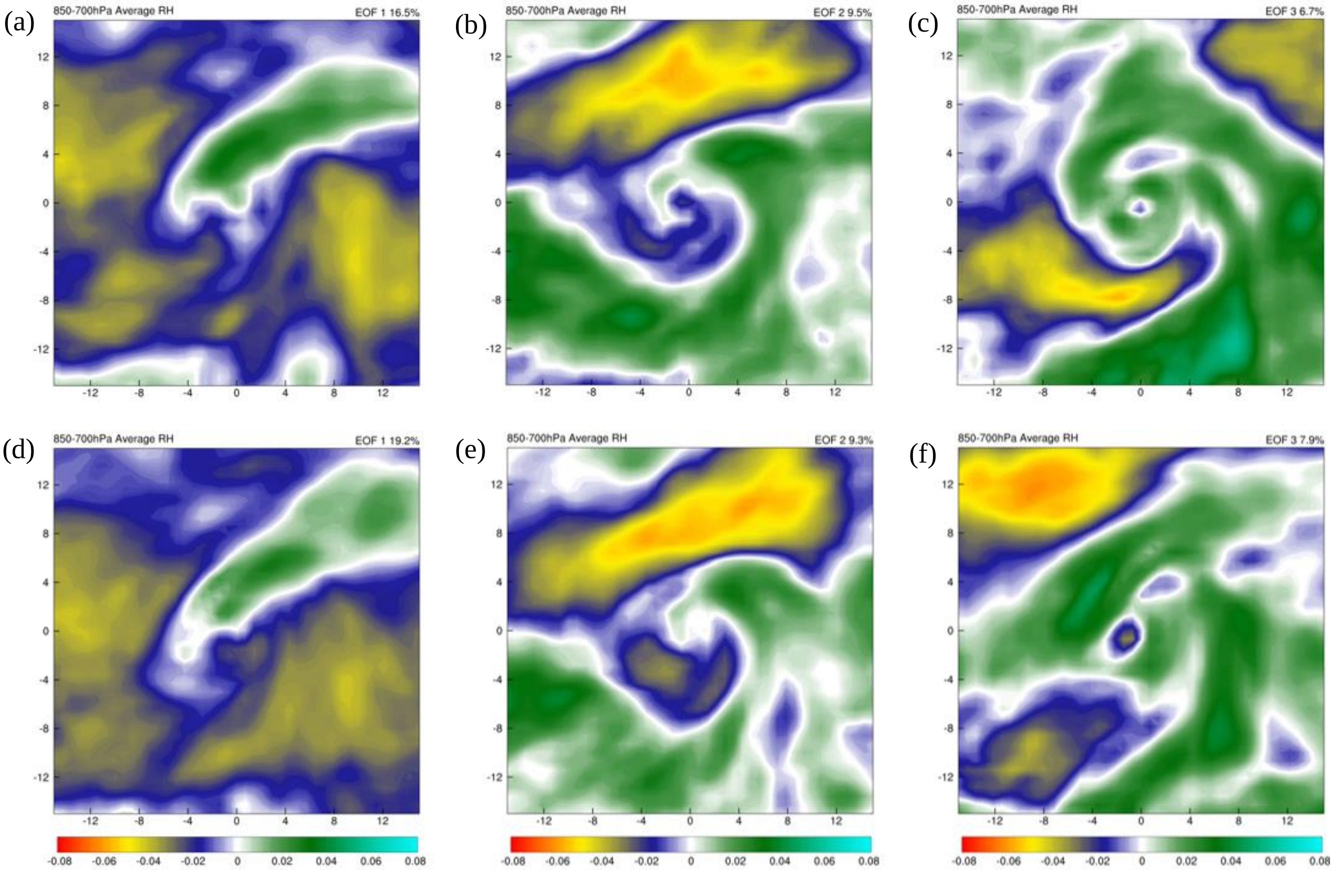


Figure 7. RH field EOF mode 1, 2, 3 for (a) ~ (c) onset of failed ERCs, and (d) ~ (f) termination of failed ERCs, respectively.

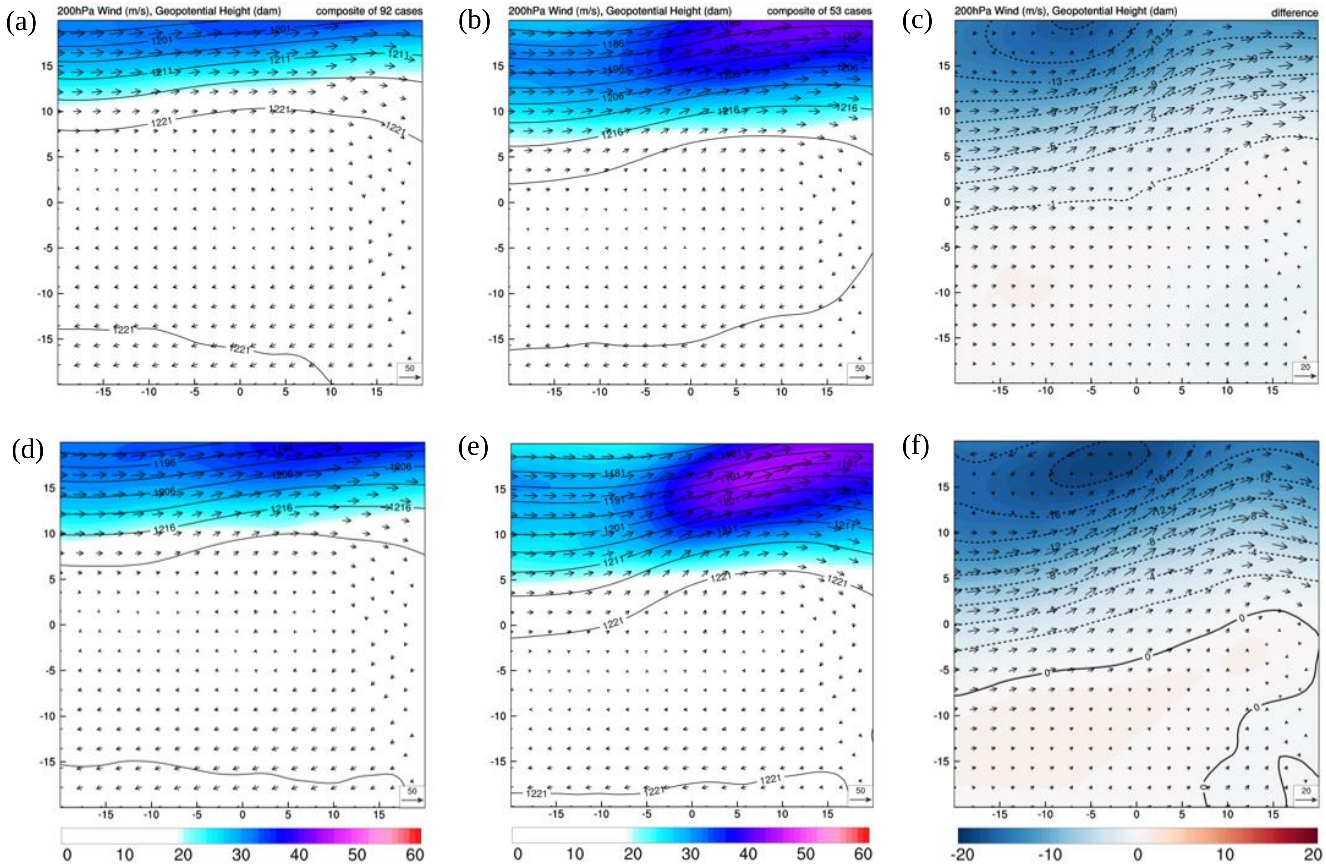


Figure 8. Composite maps of 200hPa geopotential height (dam), and wind vectors (m/s) within 20°×20° relative to TC center, for (a) onset of successful ERCs, (b) onset of failed ERCs, (d) completion of successful ERCs, (e) termination of failed ERCs. Plots on the rightmost panel are difference fields of failed cases minus successful cases at (c) ERC starting time, and (f) ERC ending time. Note the subtraction sequence is different from RH plots. Shaded area represents geopotential height difference, not wind magnitude difference.

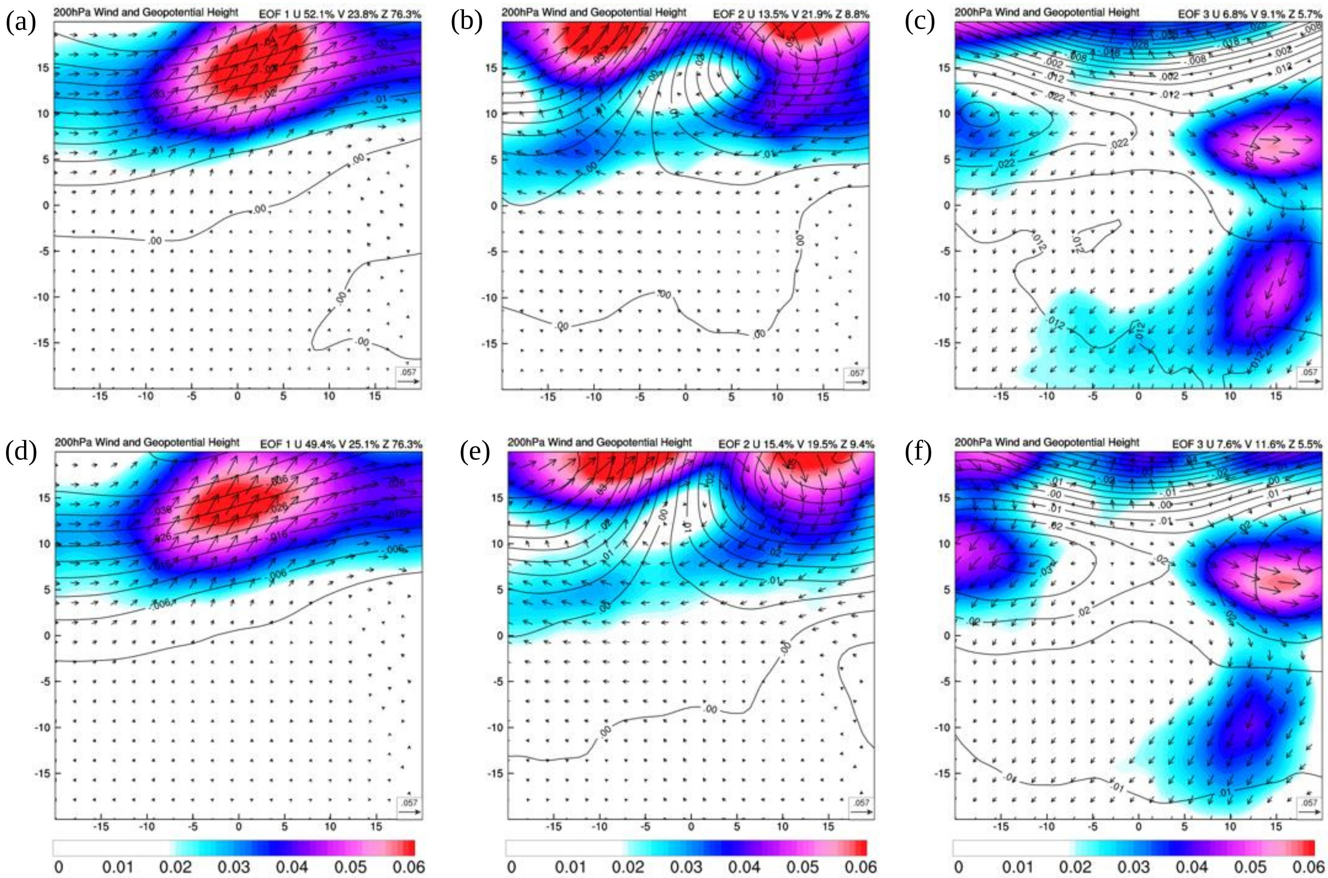


Figure 9. Z (contour), U and V (vector, shading) field EOF mode 1, 2, 3 for (a) ~ (c) onset of successful ERCs, and (d) ~ (f) completion of successful ERCs, respectively. Combination of modes from U, V field to yield vector modes is purely artificial.

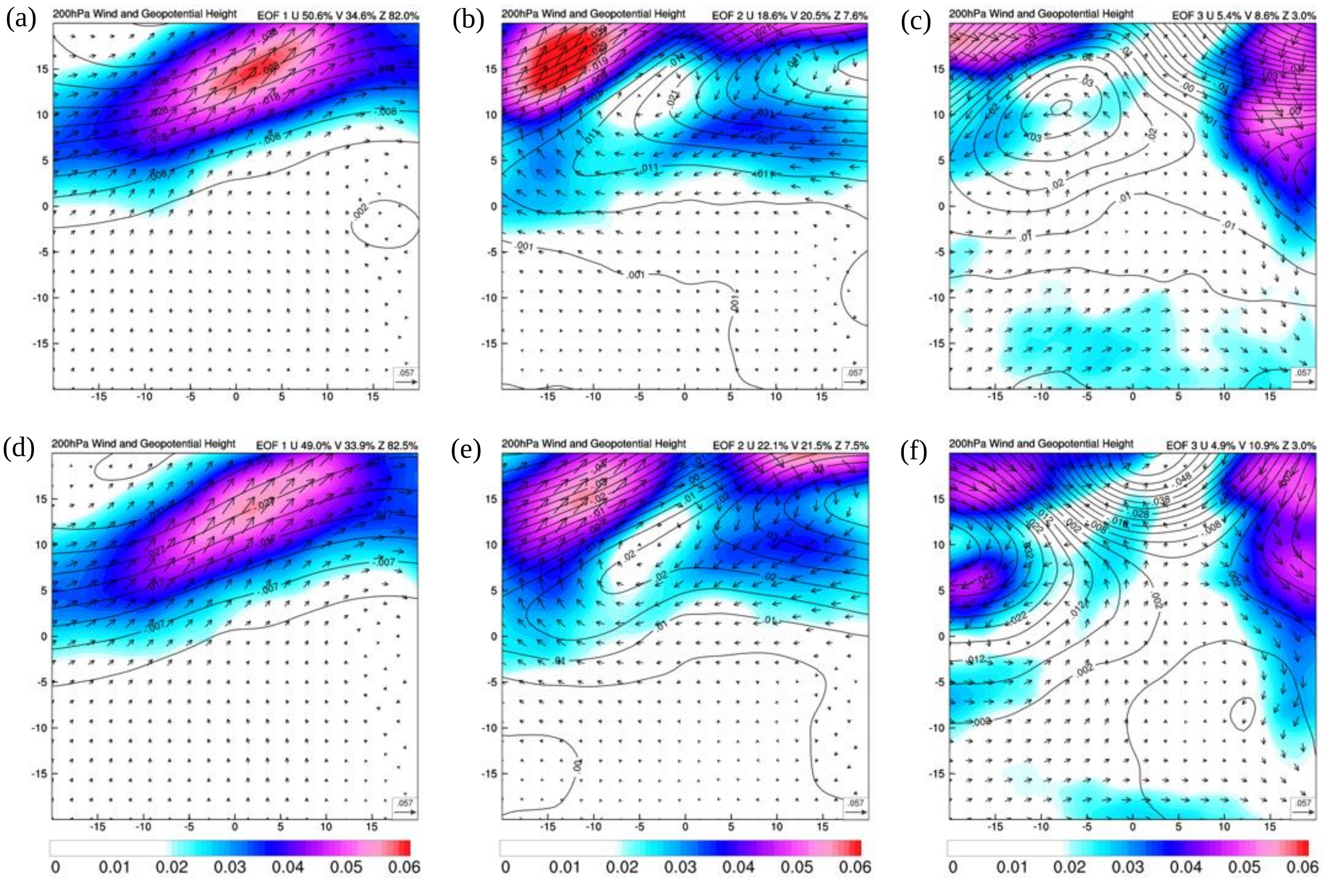


Figure 10. Z (contour), U and V (vector, shading) field EOF mode 1, 2, 3 for (a) ~ (c) onset of failed ERCs, and (d) ~ (f) termination of failed ERCs, respectively. Combination of modes from U, V field to yield vector modes is purely artificial.